Published in Chemical Engineering Science, doi: 10.1016/j.ces.2011.10.049

Mass transfer characteristics of liquid films flowing down a vertical wire in a counter current gas flow

J. Grünig*, E. Lyagin, S. Horn, T. Skale, M. Kraume

Chair of Chemical and Process Engineering, Technische Universität Berlin, Straße des 17. Juni 135, D-10623 Berlin, Germany

*Corresponding author. Address: Ackerstraße 71-76, D-13355 Berlin, Germany. Tel.: +49 30 314 72687; fax: +49 30 314 72756. Email-address: jochen.gruenig@tu-berlin.de.

Abstract: The wetted-wire packing, mainly consisting of a bundle of vertical parallel wires, is a promising concept for the use in separation columns. To investigate the multiphase flow inside the packing in detail and to estimate the performance of the packing, experiments on liquid films on a single vertical wire in a counter current gas flow were carried out. To get information about the interfacial area, an optical measurement of the film thickness was carried out with a digital high speed camera and image recognition tools. By measuring the evaporation of water and aqueous polyvinylpyrrolidone solutions into air, the gas-side mass transfer was determined. The liquid-side mass transfer was examined by measuring the desorption of CO_2 from water into air. The results show that the mass transfer coefficients are comparable to those appearing in common structured packings. When assuming a sufficiently high wire packing density, a specific interfacial area similar to corrugated sheet structured packings can be reached. Previous studies predicted a low pressure drop per packing height and extended capacity limits compared to common packings. In consideration of these results, the wetted wire packing therefore is shown to be suitable especially for absorption processes where a low pressure drop is favourable.

Keywords: Wetted wire packing, films, mass transfer, multiphase flow, absorption

1 Introduction

Packed columns are widely used in chemical industry for separation processes, in which liquid films run over the surface of structured packing elements. Available packings are optimised to achieve high separation efficiencies at a low specific pressure drop and a wide operating range. However, one problem is the liquid distribution in the packing so that the liquid has to be redistributed after a certain packing height.

Hattori et al. (1994) suggested that a packing concept consisting of bundles of parallel vertical wires would have advantages compared to conventional packings. Unlike random and regular packings, the wire packing has straight gas channels, which cause a lower pressure drop over the packing and offer higher load limits. As radial liquid transport is inhibited by the structure of the wire packing, the maldistribution of the liquid will be reduced significantly. Thus, a redistribution of the liquid is not necessary. On the other hand due to the lack of internal mixing the wire packing requires a highly uniform initial liquid distribution by a special distributor.

However, the construction and installation of the packing and the distributor pose problems that still have to be solved, although there are several design suggestions from different authors (Jödecke et al., 2008; Migita et al., 2005; Nagaoka and Manteufel, 2003; Vogelpohl, 2006). However, the crucial question is whether the separation performance of the wire packing is competitive to conventional packings, which depends on the specific surface area, the mass transfer coefficients, the operating limits and the specific pressure drop. These parameters are related to the fluid dynamics, physical properties of the particular system and the packing geometry.

To understand the behaviour of fluid dynamics and mass transfer in detail, our experiments focus on a single packing element, which is represented by one vertical wire. The aim of this study is also to estimate the performance of a wire packing and to clarify whether it would be competitive to conventional packings so that the higher technical effort can be justified.

1.1 Liquid film flow on wires and threads

Most investigations on liquid film flow are conducted with plates or tubes of large diameters compared to the film thickness so the film can be considered as planar. Fundamental theoretical studies were made by Nusselt (1916) who characterised the laminar film flow on plates. Different authors used intrusive (Brauer, 1956) and non-intrusive (Adomeit and Renz, 2000; Chu and Dukler, 1974; Helbig, 2007; Hiby, 1968; Lel et al., 2005; Mouza et al., 2000) measurement techniques to determine the film thickness and the wave velocities.

However, when the film thickness is in the same order of magnitude as the cylinder radius the curvature cannot be neglected. Rayleigh (1878) was the first to give a mathematical description of the instability of a cylindrical liquid jet that explains the formation of waves as a result of capillary forces. Grabbert and Wünsch (1973)

theoretically compared falling films on different geometries and observed the influence of curvature on the fluid dynamics of smooth films. Goren (1962) made a theoretical analysis of the instability of a liquid film on a cylinder and calculates the wavelength with the fastest growing amplitude. Since he focused on liquids of high surface tensions and viscosities and small cylinder diameters, he neglected the gravitational forces. In the work of Lin and Liu (1975) the authors also considered the gravitational forces in their theoretical model to describe the coating of wires and tubes by withdrawing them from a liquid pool. They found that the film is unstable at any set of parameters that causes the formation of waves. Trifonov (1992) calculated wavy regimes of viscous liquid films on wires. The results showed a significant influence of the curvature on the wave formation. Recent investigations on the instabilities of annular films were presented e.g. by Kliakhandler et al. (2001), Craster and Matar (2006) and Duprat et al. (2009). They performed numerical simulations as well as experiments with viscous fluids on single wires. A comparison of bead frequency and bead thickness showed a very good agreement and the simulations indicated an inner circulation in the beads at higher flow rates. Hattori et al. (1994) proposed the use of wires in gas-liquid contact devices for heat and mass transfer. They argued that due to the formation of liquid beads the contact device would have all advantages of a spray column (low pressure drop and large film surface area), but at the same time the wires reduce the velocity of the beads and therefore enhance their contact time with the gas phase. In addition, the wires induce an internal circulation in the beads which also promotes heat and mass transfer.

1.2 Mass transfer of liquid films

Most mass transport measurements on liquid films are conducted in wetted wall columns. The gas-side mass transfer rate was investigated by numerous researchers, a well-known study is that of Gilliland and Sherwood (1934) in which the evaporation of different liquids into air was observed. However, the influence of the liquid flow rate on the mass transfer rate was not investigated. Braun and Hiby (1970) studied the gas-side mass transfer with the absorption of ammonia in diluted sulphuric acid. They also considered the influence of humidity, liquid flow rate and column height. An overview of early relevant works in this field is given in a paper of Spedding and Jones (1988), further references can be found in the work of Erasmus and Nieuwoudt (2001). The rate of gas-side mass transfer of liquid films on strongly curved surfaces has not been investigated yet.

The liquid-side mass transfer of planar films has also been investigated by a large number of authors (e.g. Henstock and Hanratty, 1979; Hikita and Ishimi, 1987; Park and Nosoko, 2003; Yoshimura et al., 1996). The absorption of CO_2 into a film of water on a thin wire was investigated by Chinju et al. (2000). Grabbert (1974) studied the absorption of CO_2 in water films on cylinders of different diameters and observed that the mass transfer is enhanced by increasing curvature of the surface. Uchiyama et al. (2003) used the same test facility as Chinju et al. (2000) to carry out measurements on the absorption of CO_2 into aqueous monoethanolamine solutions. Migita et al. (2005) built a prototype of a wetted wire column in laboratory scale and performed mass transfer experiments with the model systems used by Uchiyama et al. (2003). In a similar wetted wire column, Pakdehi and Taheri (2010) measured the separation of hydrazine from an air flow with water. In both works the results were compared with a random packing column and it revealed that comparable mass transfer rates at a significantly lower pressure drop could be achieved. In all the above mentioned experiments the gas load was comparatively low and an interaction of liquid and gas phase fluid dynamics was not observed. Mass transfer experiments at high gas and liquid Reynolds numbers were carried out by Nielsen et al. (1998) in a wetted wall column in concurrent flow.

For the wire geometry, there is no data available in the liquid and gas load range in which packed columns are usually operated. Thus, there is still a lack of experimental data for highly curved geometries in the operating range where the gas phase affects the liquid flow. It is the aim of this study to measure the relevant parameters for packed column characterisation in the appropriate parameter range. This work follows a previous study (Grünig et al., 2010) which focussed on the fluid dynamics of the on-wire film flow using the present test facility. On the basis of the previous investigations, the current paper discusses mass transfer experiments carried out with different liquids. As the effective surface area for mass transfer is calculated from fluid dynamic data, results of optical measurements for these liquids are also presented in this paper.

2 Methods and materials

2.1 Experimental set-up

The flow sheet of the experimental set-up is shown in Fig. 1 [**Fig. 1.** Sketch of experimental set-up.]. The main element is a vertical glass channel with a quadratic

cross sectional area of 20 mm × 20 mm and a length of 1 m. A round wire of stainless steel with a diameter of 1 mm is fixed in its centre. Liquid is pumped from a storage tank to the top of the channel with a gear pump (BVP-Z, Ismatec GmbH). The liquid is distributed on the wire inside the channel head and flows down as an annular film and gets into contact with the gas phase. The gas/liquid contact length is 1040 mm. At the channel bottom, the liquid is collected and fed back into the storage tank. An alternative liquid routing (Fig. 1 b) is used for the liquid-side mass transfer measurements (see Section 2.3). Air is guided in the bottom of the channel and flows upwards counter currently to the liquid film before it exits into the environment. The inlet temperatures of liquid and gas phase are regulated by heaters and measured at the in- and outlet of the channel. A high speed camera and a synchronised lighting are used to detect the film thickness and the bead velocity at different vertical positions. The analysis of the images is automated with an image recognition software tool (Image ProPlus V.5). A more detailed description of the test facility and the optical measurement methods is given in (Grünig et al., 2010).

2.2 Gas-side mass transfer

The mass transfer coefficients are mean values, which are averaged over the channel length. It is assumed that the length to diameter ratio of the channel is large enough that the mean mass transfer coefficients are valid for long running lengths.

The gas-side mass transfer was determined by the rate of evaporation from the liquid into the gas phase. A dew point hygrometer (DPS1, EdgeTech Co.) is used to measure the humidity of air at the outlet. Before each measurement run the inlet air humidity is measured with the channel under dry conditions. The dew point temperatures were measured in a range of -25 °C (gas inlet) and -2 °C at a pressure of 1.013×10^5 Pa with an accuracy of ± 0.25 °C. Due to the effect of the evaporation enthalpy, the difference of the liquid inlet and outlet temperature reached up to 9 °C. Water and aqueous polyvinylpyrrolidone (PVP) solutions were used as liquids. The addition of PVP (PVP powder K90, AppliChem GmbH) intended to increase the viscosity of the liquid and preliminary investigations revealed that it had a negligible influence on the vapour pressure in the observed concentration range. This also means that even though there is a concentration gradient in the film due to the evaporation of the water, the vapour pressure at the phase interface is not influenced. Therefore a liquid side resistance for mass transfer can be neglected. Since the evaporation rate is much lower than the liquid

flow rate (< 1 %) and the bead motion provides an intensive mixing, the concentration profile in the film should be relatively even and the local viscosity should not change significantly.

The liquid properties are listed in Tab. 1 [**Tab. 1.** Physical properties of the investigated systems at 20 °C.]. The viscosities of the PVP solutions were measured with a rotational viscometer (VT 550, Haake GmbH). Measurements at different shear rates showed the Newtonian behaviour of the PVP solutions. A pendant drop type tensiometer was used to measure the surface tension of the PVP solutions.

Tab. 1. Physical properties of the investigated systems at 20 °C.

	ρ [kg/m³]	η [mPa s]	σ [mN/m]		D [m²/s]
Water	998[b]	1.0[b]	72.7[a]	Water-CO_2	1.79×10^{-9} [d]
3 wt % aq. PVP sol. (PVP3)	1009[c]	11.8[c]	68.0[c]	Air-water	2.44×10^{-5} [e]
6 wt % aq. PVP sol. (PVP6)	1016[c]	49.0[c]	68.3[c]		

[a] Wohlfarth and Wohlfarth (1997), [b] VDI-Wärmeatlas (1994), [c] Own measurements, [d] Wilke and Chang (1955), [e] Fuller et al. (1966).

The evaporation flow rate of water $\dot{N}_{H2O}$ is determined by a molar balance based on the molar fractions of the inlet and outlet gas flow:

$$\dot{N}_{H_2O} = \dot{N}_{g,in} \frac{y_{H_2O,out} - y_{H_2O,in}}{1 - y_{H_2O,out}}. \quad (1)$$

The molar fractions are calculated from the humidity of the air with is measured with the hygrometer. With the assumption of the validity of the ideal gas law, the mean logarithmic concentration difference can be formulated in terms of partial pressures at the gas inlet and outlet as

$$\Delta p_{H_2O,ln} = \frac{(p_{H_2O,I} - p_{H_2O})_{in} - (p_{H_2O,I} - p_{H_2O})_{out}}{\ln \frac{(p_{H_2O,I} - p_{H_2O})_{in}}{(p_{H_2O,I} - p_{H_2O})_{out}}}. \quad (2)$$

The partial pressures $p_{H2O,I}$ at the interface are the saturation vapour pressures at liquid temperature, which are determined with the Magnus equation according to VDI 3514 Part 1 (2007). With this information, the mean gas-side mass transfer coefficient is calculated as follows:

$$\beta_g = \frac{\dot{N}_{H_2O} \cdot R \cdot T_{g,m}}{p \cdot A_{l,W}} \cdot \frac{p_{air,m}}{\Delta p_{H_2O,ln}}. \quad (3)$$

This equation considers the Stefan diffusion according to Gilliland and Sherwood (1934) where $p_{air,m}$ is the mean partial pressure of the inert gas (air) which is calculated as

$$p_{air,m} = p - \frac{p_{H_2O,I,in} + p_{H_2O,I,out} + p_{H_2O,in} + p_{H_2O,out}}{4}. \quad (4)$$

2.3 Liquid-side mass transfer

The liquid-side mass transfer was determined by measuring the desorption of CO_2 from water into air. Water was enriched with CO_2 from a gas bottle. Unlike as for gas-side mass transfer measurements, the liquid was not recycled but drained into a collecting tank (Fig. 1 b). The storage tank was replaced by a 5 L plastic bag so the gas phase could be removed completely. By this means the desorption of CO_2 from the liquid before entering the channel was avoided. Liquid samples were taken from the inlet and outlet of the channel and were analysed for their CO_2 concentration.

To determine the concentration of CO_2 in the liquid, samples of a defined volume $V_{l,Probe}$ = 100 mL were stripped in a washing flask with air which was guided to a gas analyzer (S710, Maihak GmbH) afterwards. Volume flow rate, temperature, pressure and the gas molar fraction of CO_2 of the gas flow were recorded over time. Before a liquid probe is put into the washing flask, the molar fraction stays at a constant value of $\bar{y}_{CO2} \approx 400$ ppm which is the value of air. The addition of the liquid probe causes a peak in the gas molar fraction which falls back to the initial value $\bar{y}_{CO2}$. The amount of CO_2 that was stripped from the probe can be determined by the peak area similar to a gas chromatogram:

$$N_{CO_2,strip} = \int_0^t (y_{CO_2}(t) - \bar{y}_{CO_2}) \dot{N}_g dt. \quad (5)$$

The molar flow rate of air is calculated with the ideal gas law:

$$\dot{N}_g = \frac{p_g \dot{V}_g}{T_g R}. \quad (6)$$

Since the air has an initial content of CO_2, the liquid sample is stripped to the correspondent liquid equilibrium concentration which is described by Henry's law (H = 1417 bar at 20 °C (Harvey, 1996)):

$$\bar{x}^*_{CO_2} = \frac{p\,\bar{y}_{CO_2}}{H}. \tag{7}$$

Because $\bar{x}^*_{CO2}$ is relatively small, the concentration of the liquid probe can be evaluated as

$$\bar{c}^*_{CO_2} \approx \bar{x}^*_{CO_2}\,\frac{\rho_l}{\tilde{M}_l}. \tag{8}$$

The mean concentration of CO_2 in the probe can then be determined by

$$\bar{c}_{CO_2} = \frac{N_{CO_2,strip}}{V_{l,Probe}} + \bar{c}^*_{CO_2}. \tag{9}$$

The mean liquid-side mass transfer coefficient is calculated as

$$\beta_l = \frac{\dot{V}_l(\bar{c}_{CO_2,in} - \bar{c}_{CO_2,out})}{A_{l,W}\,\Delta\bar{c}_{ln}}, \tag{10}$$

whereas the logarithmic concentration difference is given by

$$\Delta\bar{c}_{ln} = \frac{(\bar{c}_{CO_2} - c^*_{CO_2})_{in} - (\bar{c}_{CO_2} - c^*_{CO_2})_{out}}{\ln\dfrac{(\bar{c}_{CO_2} - c^*_{CO_2})_{in}}{(\bar{c}_{CO_2} - c^*_{CO_2})_{out}}}. \tag{11}$$

The equilibrium concentrations c^*_{CO2} of the liquid are calculated with Henry's law from the correspondent CO_2 concentrations in the gas phase at the inlet and outlet of the channel. While the inlet concentration was directly measured with the gas analyser, the outlet concentration was calculated by a molar balance over the gas phase. An analysis of error determined an overall measurement error of the liquid-side mass transfer coefficient of ± 6 %.

3 Results and discussion

3.1 Fluid dynamics of the film flow

Film thickness

Water gives an irregular film profile of differently sized beads running with varying velocities. However, at low liquid and gas flow rates, PVP6 shows a regular pattern of evenly sized beads running with the same velocity. As the gas load increases, the flow becomes irregular. Figs. 2 a) and b) [**Fig. 2.** Recording of the local film for a) no gas load and b) high gas load.] show this behaviour as film thickness recordings at two different gas loads. Corresponding image captures of the liquid film are shown in Fig. 3 a) and b)

[**Fig. 3.** Pictures of the liquid film of PVP6, B_W = 0.19 m³/(m h) for a) no gas load and b) high gas load. c): Sketch of film volume model.] The beads appear as peaks in the film thickness profile and can clearly be distinguished from the basis film. When plotting the mean values of the basis film and bead thickness against the gas load (Fig. 4 a) and 4 b)) [**Fig. 4.** Mean basis film thickness (a), mean bead thickness (b), and mean bead frequency (c) against the gas load for different liquids.], it reveals that the basis film thickness does not change significantly as the gas load increases. But as the liquid viscosity increases, the basis film thickness rises. In contrast to the basis film the bead thickness rises with increasing gas load. This is because the bead volume increases and the beads are forced into a more compact shape (see Figs. 3 a) and b)). The increased accumulation of liquid volume in the beads at higher gas loads is also indicated by decreasing bead frequencies for all liquids (Fig. 4 c). These results agree with previous findings from Grünig et al. (2010). The sudden change of basis film and bead thickness for PVP6 at a gas load of F_C = 5.6 Pa$^{0.5}$ seen in Fig. 4 a) and b) can be explained by the transition from regular to irregular flow (see also Figs. 2 a) and b)).

Mean bead velocity

In Fig. 5 [**Fig. 5.** Mean bead velocity depending on the gas load for different liquids and liquid loads.] the mean bead velocity is plotted over the gas load for different liquids and liquid loads. The velocity of the beads is not influenced by the gas load. This means that the beads are not decelerated by the gas flow although they change their shape. With decreasing viscosity and increasing liquid loads higher bead velocities are achieved. The error bars show the large deviation of the velocities from the mean value in the case of irregular flow as for water with B_W = 0.76 m³/(m h). For flow conditions with regular beads the bead velocity fluctuations are very small, like for PVP6 with B_W = 0.19 m³/(m h).

Interfacial area

Fig. 6 [**Fig. 6.** Specific interfacial area depending on the gas load for different liquids and liquid loads.] shows the specific interfacial area $\tilde{a}_{l,w}$ of a single wire for different liquids and liquid loads over the gas load. The interfacial area was calculated according to the film volume model shown in Fig 3 c) involving the film thickness and bead velocity data (more details are given in (Grünig et al., 2010)). It appears that the effective film surface area is significantly higher than the specific surface of the dry wire $\tilde{a}_W$. Although the

bead thickness rises with increasing gas load, the results indicate that the gas load has no significant influence on the film surface area. However, it becomes apparent that the interfacial area increases both with rising viscosity and liquid load.

Liquid hold-up

In Fig. 7 [**Fig. 7.** Liquid hold-up depending on the gas load for different liquids and liquid loads.] the liquid hold-up depending on the gas load for different liquids and liquid loads is plotted. It is also calculated from the geometric film volume model presented in Fig. 3 c). The liquid hold-up rises with increasing viscosity and liquid load but is only slightly influenced by the gas load. This is similar to the behaviour of packed columns for conditions below the loading point.

In summary it can be said that the interfacial area and the liquid hold-up are not significantly affected by the gas flow. An increasing gas load causes the liquid to distribute across larger beads. With the overall liquid hold-up remaining constant this means that the distance between the beads increases at higher gas loads. This is consistent with the observation that the bead frequency decreases with rising gas load while the bead velocity remains constant (Grünig et al., 2010).

3.2 Gas-side mass transfer

In Fig. 8 [**Fig. 8.** Gas-side mass transfer coefficient depending on the gas load for different liquids and liquid loads. Experimental values are compared to theoretical values calculated with the penetration theory.] the gas-side mass transfer coefficients which are related to the interfacial area are plotted against the gas load for different liquids and liquid loads. As the gas load rises, the mass transfer coefficients increase. It appears that the mass transfer coefficients also increase with decreasing liquid viscosity. This is probably caused by higher bead velocities at lower viscosities resulting in increased relative velocities between beads and gas phase. When comparing different liquid loads, the PVP-solutions show minimal difference in mass transfer coefficients at lower gas load. At higher gas loads the mass transfer is enhanced for higher liquid loads. However, the mass transfer coefficients of water deviate significantly for different liquid loads over the whole gas load range. The clear dependency on the liquid load can be explained by the enhancement of turbulence in the gas flow due to the increased waviness of the liquid film with rising liquid loads.

Theoretical values of the mass transfer coefficient calculated with the penetration theory from Higbie (1935) as

$$\beta_g = \frac{2}{\sqrt{\pi}} \sqrt{\frac{D_g}{\tau}} \tag{12}$$

are also added to the diagram. The contact time τ was chosen to be the surface contact time of a gas volume element between two beads. The mean bead distance is calculated from the mean bead velocity and frequency

$$s_B = \overline{w}_B / f_B \tag{13}$$

so the contact time is depending on the relative velocity of gas and beads:

$$\tau = s_B / (\overline{w}_{gC} + \overline{w}_B). \tag{14}$$

Although the theoretical values are higher than the experimental, the dependency of the gas load is in quite good agreement. The influence of the liquid load on the mass transfer coefficients shows the same tendency as the experiments, but the effect is more pronounced in theory. This is because the distance between the beads decreases significantly with increasing gas load, which leads to shorter contact times. However, the penetration theory in combination with the chosen contact time definition fails to predict the influence of the liquid viscosity on the mass transfer. With increasing viscosity, the bead distance decreases, which results in the prediction of higher mass transfer coefficients while the experiments showed that the mass transfer coefficients decrease with increasing viscosity. Thus, the flow regime seems to be too complex for the prediction of mass transfer coefficients in all cases with the chosen parameters.

In Figs. 9 a) and b) [**Fig. 9.** Mean gas-side Sherwood number depending on the Reynolds number for different liquids and different liquid loads a) and b). Comparison with correlations for mass transfer in tubes (Braun and Hiby, 1970) and inside structured packings (Bravo and Fair, 1982).] the Sherwood-number for gas-side mass transfer is plotted against the Reynolds number for different liquids and two different liquid loads. A correlation from Braun and Hiby (1970) for the gas-side mass transfer of liquid films in tubes in counter current configuration is added to the diagrams:

$$Sh_g = 0.015\, Re_g^{0.4}\, Re_l^{0.16}\, Sc_g^{0.44}\, (1 + 5.2 (L_W / b_C)^{-0.75}). \tag{15}$$

Additionally, a general correlation for the gas-side mass transfer inside the gas passages of structured packings is added (Bravo and Fair, 1982), which is independent from the liquid load and liquid properties

$$Sh_g = 0.0388\, Re_g^{0.8}\, Sc_g^{0.333}. \quad (16)$$

It is apparent that the mass transfer of the wire film flow is higher for all liquids and liquid loads compared to the film flow inside tubes. This can be seen as an effect of the higher waviness and higher relative velocity of the phases causing enhanced turbulence in the gas flow and thus increasing the mass transfer. On the other hand, the geometry itself should also have an influence on the mass transfer. Compared to planar films, higher gas velocity gradients develop at the film surface due to its curvature and this should also enhance the mass transfer. For higher liquid loads (Fig 9 a)), the mass transfer for the PVP-solutions is in quite good agreement compared to the structured packing correlation, which indicates that a similar grade of turbulence as in the gas passages of packings is reached. In the case of water, the mass transfer even exceeds that of the packing correlation. At lower liquid loads (Fig 9 b)), the PVP-solutions show lower mass transfer at higher gas loads compared to the structured packing correlation, whereas the mass transfer characteristic of water is only slightly higher than the packing correlation.

In summary, it can be said that the viscosity has a visible influence on the mass transfer, which can be explained by its impact on the waviness of the flow and the bead velocity. The mass transfer rates are in the same order of magnitude compared to those achieved in structured packings. However, it has to be mentioned that the gas passages in a structured packing are tortuous which increases the effective phase velocities. This is considered in the model of Rocha et al. (1996) where the influence of different inclination angles of corrugated sheet packings on the mass transfer is discussed.

3.3 Liquid-side mass transfer

The results of the liquid-side mass transfer measurements with the CO_2-water/air system are shown in Fig. 10 [**Fig. 10**. Liquid-side mass transfer coefficient depending on the gas load for different liquid loads. Comparison with data derived from Brauer (1971) for planar films (independent from gas load) and the model of Rocha et al. (1996) for structured packings.]. As a reference, an empirical correlation

$$Sh_l = C\, Re_l^a\, Sc_l^{0.5} \text{ with}$$
$$C = 0.0224,\ a = 0.8 \text{ for } Re_l = 12 - 70 \text{ and} \quad (17)$$
$$C = 0.08,\ a = 0.5 \text{ for } Re_l = 70 - 400$$

given by Brauer (1971) for liquid films on planar surfaces which is not dependent on the gas load is added to the diagram. Additionally, gas-side mass transfer coefficients as they appear in structured packings calculated with the model of Rocha et al. (1996) (a_p = 200 m²/m³, φ = 45 °) are shown in the diagram. It is apparent that the mass transfer coefficients of the wire film flow are higher and show a greater dependency of the liquid load than for planar films. This indicates that the internal mixing of the liquid film is enhanced by the bead formation of the film. Furthermore, an increasing film curvature also enhances the mass transfer compared to a planar film as Grabbert (1974) showed in a theoretical examination. The results also indicate that increasing gas load raises the liquid-side mass transfer. The predicted mass transfer coefficients in structured packings according to Rocha et al. (1996) are higher than the experimental values but show also a strong liquid load dependency. Unlike for the wire film flow, the mass transfer coefficients for structured packings decrease with increasing gas load. The model uses the penetration theory and calculates the contact time with the packing corrugation length and the mean film velocity. Since the film velocity decreases with increasing gas load, higher contact times are obtained leading to lower liquid-side mass transfer coefficients.

In Fig. 11 [**Fig. 11.** HTU_l values for the single wire depending on the liquid flow rate for different gas loads. Comparison with data from Chinju et al. (2000).] the height of a transfer unit HTU_l for the single wire is plotted over the liquid load for different gas loads (see Appendix A). For comparison, the data of Chinju et al. (2000) is added to the diagram which has been modified according to Appendix B. Chinju et al. (2000) performed single wire experiments at lower gas and liquid load, but the trend seems to fit to our experimental data. The increase of the liquid-side mass transfer coefficient with rising gas load (see Fig. 10) leads to the decrease of the HTU_l values.

4 Estimation of wetted wire packing separation performance

To estimate the packing behaviour from the single-wire data it must be considered that the packing has a lower void fraction than the test channel. When we assume equal effective mean gas velocities in both the packing and the channel, the superficial gas velocity in the packing has to be lower. This behaviour is expressed by

$$F_P = \frac{\varepsilon_P (1 - h_{l,P})}{\varepsilon_C (1 - h_{l,C})} F_C . \tag{18}$$

The packing liquid load defined as the total liquid flow rate referred to the cross sectional area of the packing. This means that the flow rate on a single wire $\dot{V}_{\mathrm{l,W}}$ has to be multiplied with the number of wires per cross sectional area of the packing:

$$B_{\mathrm{P}} = \dot{V}_{\mathrm{l,W}} z_{\mathrm{P}}. \tag{19}$$

4.1 Effective surface area

An estimation of the fluid dynamics was already presented in (Grünig et al., 2010). One important aspect for the estimation of the mass transfer is the effective film surface area in the packing. Another parameter is the liquid hold-up, which accounts for the restriction of the cross sectional area for the gas flow. Both values are taken from the single wire measurements and are used to predict the mass transfer performance of a packing with a certain wire packing density. The specific effective interfacial area of the packing is calculated as

$$a_{\mathrm{l,P}} = \widetilde{a}_{\mathrm{l,W}} z_{\mathrm{P}}. \tag{20}$$

Fig. 12 [**Fig. 12.** Predicted effective film surface area depending on the packing liquid load for different wire packing densities.] shows the calculated effective film surface area in dependency of the packing liquid load for different wire packing densities. Since the film surface area and the liquid hold-up show no dependency of the gas load in the measured range, mean values were used in the calculation. The values for the dry packing surface area depending on the wire packing density are also plotted in the diagram. A common value for the specific packing surface of corrugated sheet packings is $a_{\mathrm{P}} = 250\ \mathrm{m^2/m^3}$, but there also exist packings with much higher values. To be comparable to structured packings in this respect a wire packing density of $z_{\mathrm{P}} = 62{,}500$ wires/m^2 (the pitch would be 4 mm in a quadratic pattern) seems to be reasonable which gives a specific dry surface area of $a_{\mathrm{P}} = 196\ \mathrm{m^2/m^3}$. It is apparent that the effective surface area rises with increasing liquid load and exceeds the dry packing area significantly. This is caused by the increasing film surface area on the individual wires due to increasing film radii. However, when considering the liquid film on corrugated sheet packings as planar, a higher film thickness should not affect the film surface area from a geometrical perspective. A recent study of Aferka et al. (2011) showed that the

effective interfacial of a structured packing rises slightly with increasing liquid load but does not exceed the dry packing surface area.

4.2 Gas-side separation efficiency

Fig. 13 [**Fig. 13.** Predicted HTU_g values depending on the gas load for different liquids and liquid loads and a defined wire packing density.] shows the predicted HTU_g values depending on the gas load for different liquids and liquid loads. It becomes apparent that the HTU_g values increase with rising gas load. The HTU_g values decrease with increasing liquid load; this is mainly due to the strong dependency of the effective surface area on the liquid load as already shown in Fig. 6. For the same reason, the HTU_g values are decreasing with increasing liquid viscosity since higher film thicknesses lead to larger effective surface areas. This effect is stronger than the decreasing gas-side mass transfer coefficients with increasing liquid viscosity. In other words, the volumetric mass transfer coefficients $\beta \cdot a_{l,P}$ rise with increasing liquid viscosity.

Fig. 14 [**Fig. 14.** Predicted HTU_g values of the packing depending on the gas load for different liquid loads for a defined wire packing density in comparison with literature data.] shows the HTU_g values depending on the gas load for different liquid loads for the system water/air. For comparison, the HTU_g values for a corrugated sheet packing (a_p = 200 m²/m³, φ = 45 °) calculated with the model of Rocha et al. (1996) as well as data for the overall HTU_{og} values of a Ralu-Pak 250YC packing (a_p = 250 m²/m³, φ = 45 °) (Maćkowiak, 1999) are included. It is predicted that the wire packing can be operated at higher gas loads than corrugated sheet packings. The higher HTU_g values of the wire packing show that the gas-side separation efficiency is worse than for structured packings of comparable specific surface area. The main reason is that the inclination of the gas channels causes higher effective gas velocities in the corrugated sheet packing. This leads to higher gas-side mass transfer rates compared to the wire packing where the gas passages are straight. This effect also becomes apparent when comparing the separation efficiency of packings with different corrugation angles. An example of the separation efficiency characteristic for a structured packing is given by the data of the Ralu-Pak 250 YC. It shows the typical increase of the efficiency at the beginning of the loading zone ("efficiency hump"). It is caused by a change in the flow regime where the mass transfer is intensified by a complex interaction between gas and liquid phase. This behaviour is neither predicted by the model data of Rocha et al. (1996), nor indicated by the predicted values for the wire packing from the single wire

experiments. But it seems possible that an interaction of the film flow on neighbouring wires in the wire packing could have a similar effect. To study this behaviour, further experiments with wires bundles have to be performed.

4.3 Liquid-side separation efficiency

In Fig. 15 [**Fig. 15.** Predicted HTU_l values depending on the gas load for different liquid loads. Comparison with the model of Rocha et al. (1996) with parameters a_p = 200 m²/m³, φ = 45 °.] the liquid-side HTU_l values of the wire packing depending on the gas load for different liquid loads are presented. Also included are the HTU_l values from the model of Rocha et al. (1996) for a corrugated sheet packing of comparable specific surface area (see section 4.2). The HTU_l values of the wire packing are comparable to those of the structured packing. Naturally, both wire and structured packing show decreasing separation efficiency with increasing liquid load. However, the wire packing has a lower decline since the specific surface area rises with increasing liquid load. Since the liquid-side mass transfer coefficients rise with increasing gas load (see Fig. 10), there is an enhancement of separation efficiency for the wire packing as well. The results indicate that the wire packing can be operated at higher gas loads than structured packings with similar liquid-side separation efficiencies.

5 Conclusions

The results of the single wire measurements show that gas-side and liquid-side mass transfer coefficients are slightly higher compared to those of planar liquid film flow, which can be ascribed to the higher waviness of the film. Due to its strong curvature, the interface area depends significantly on the liquid load and is always higher than the dry wire surface area.

The predictions show that similar values of the specific effective area of a wire bundle packing compared to common structured packings can be reached provided a sufficient wire packing density is applied. The results of this investigation indicate that a wetted wire packing does not have its benefits in applications with gas-side mass transfer controlled systems like distillation processes. However, the application of a wetted wire packing is promising in liquid-side restricted mass transfer systems like in absorption processes where a low pressure drop is of major concern. Further benefits of this packing would be the high operating range, the uniform liquid distribution and its ability to tolerate liquids of higher viscosity.

If the technical challenges in the construction can be solved satisfactorily the wire packing could be an interesting alternative in industrial applications with the above named specifications.

Acknowledgement

The authors gratefully acknowledge the financial support of the Deutsche Forschungsgemeinschaft DFG (German Research Foundation) for this work (Project no. KR1639/13-1).

Nomenclature

A	area, m^2
$A_{l,W}$	effective film surface area on wire, m^2
$a_{l,P}$	specific effective interfacial area in the packing, m^2/m^3
$\tilde{a}_{l,W}$	specific film surface area on wire, referred to wire length, m^2/m
$\tilde{a}_W$	specific surface area of dry wire, referred to wire length, m^2/m
a_P	specific surface area of the dry packing, m^2/m^3
b_C	cross sectional dimension of the channel, m
$B_P = \dot{V}_l/A_{P,CSA}$	specific liquid load in the packing, referred to cross sectional area, $m^3/(m^2\ h)$
$B_W = \dot{V}_{l,W}/C_W$	liquid load of wire, referred to the wire circumference, $m^3/(m\ h)$
c	molar concentration, mol/m^3
C_W	circumference of wire, m
D	diffusion coefficient, m^2/s
d_h	hydraulic diameter of the gas passage, m
d_W	diameter of wire, m
E	absorption efficiency, -
$F = v_g\ \rho_g^{0.5}$	gas load, F-factor, $Pa^{0.5}$
f_R	Recording frequency, 1/s
f_B	bead frequency, 1/s
H	Henry's law coefficient, bar
h	segment height, m
$h_l = V_l/(\varepsilon\ V_{tot})$	liquid fill factor, -
H_P	total packing height, m
HTU	height of a transfer unit, m

$HU_l = V_{l,W}/L_W$	liquid hold-up referred to wire length, mL/m
L_W	length of wire, m
$\tilde{M}$	molar mass, g
N	amount of substance, mol
$\dot{N}$	molar flow rate, mol/s
NTU	number of transfer units, -
p	total pressure, Pa
p_A	partial pressure of component A, Pa
p_{BM}	mean partial pressure of inert component B, Pa
R	universal gas constant, J/(mol K)
$Re_g = \bar{w}_g d_h/\nu_g$	gas Reynolds number, -
$Re_l = B_W/\nu_l$	liquid Reynolds number, -
$Sc_g = \nu_g/D_g$	gas Schmidt number, -
$Sc_l = \nu_l/D_l$	liquid Schmidt number, -
$Sh_g = \beta_g d_h/D_g$	gas Sherwood number, -
$Sh_l = \beta_l \delta/D_l$	liquid Sherwood number, -
s_B	distance between consecutive beads, m
T	temperature, K
t	time, s
v	superficial velocity, m/s
$\dot{V}$	volume flow rate, m^3/s
V	volume, m^3
$\bar{w}_B$	mean bead velocity, m/s
$\bar{w}_{g,C}$	mean gas velocity in the channel, m/s
x	liquid molar fraction, -
y	gas molar fraction, -
z	vertical coordinate, m
z_P	packing density of wires per cross sectional area, $1/m^2$

Greek letters

β	mass transfer coefficient, m/s
δ	film thickness, μm
ε	voidage, -

η	dynamic viscosity, Pa s
φ	corrugation angle, °
ν	kinematic viscosity, m^2/s
ρ	density, kg/m^3
σ	surface tension, N/m
τ	contact time, s

Sub- and superscripts

*	equilibrium
B	bead
BF	basis film
C	channel
CSA	cross sectional area
g	gas
I	interphase
l	liquid, wetted
ln	logarithmic
m, -	mean
P	packing
strip	stripping gas
tot	total
W	wire

References

Adomeit, P., Renz, U., 2000. Hydrodynamics of three-dimensional waves in laminar falling films. International Journal of Multiphase Flow 26, 1183-1208.

Aferka, S., Viva, A., Brunazzi, E., Marchot, P., Crine, M., Toye, D., 2011. Tomographic measurement of liquid hold up and effective interfacial area distributions in a column packed with high performance structured packings. Chemical Engineering Science 66, 3413-3422.

Brauer, H., 1956. Strömung und Wärmeübergang bei Rieselfilmen (in German). VDI-Verlag, Düsseldorf.

Brauer, H., 1971. Stoffaustausch einschließlich chemischer Reaktionen (in German). Sauerländer, Aarau.

Braun, D., Hiby, J.W., 1970. Der gasseitige Stoffübergangskoeffizient am Rieselfilm (in German). Chemie Ingenieur Technik 42, 345-349.

Bravo, J.L., Fair, J.R., 1982. Generalized Correlation for Mass-Transfer in Packed Distillation-Columns. Industrial & Engineering Chemistry Process Design and Development 21, 162-170.

Chinju, H., Uchiyama, K., Mori, Y.H., 2000. "String-of-Beads" Flow of Liquids on Vertical Wires for Gas Absorption. AIChE Journal 46, 937-945.

Chu, K.J., Dukler, A.E., 1974. Statistical Characteristics of Thin, Wavy Films: Part II. Studies of the Substrate and its Wave Structure. AIChE Journal 20, 695-706.

Craster, R.V., Matar, O.K., 2006. On viscous beads flowing down a vertical fibre. Journal of Fluid Mechanics 553, 85-105.

Duprat, C., Ruyer-Quil, C., Giorgiutti-Dauphine, F., 2009. Spatial evolution of a film flowing down a fiber. Physics of Fluids 21, doi: 10.1063/1.3119811.

Erasmus, A.B., Nieuwoudt, I., 2001. Mass transfer in structured packing: A wetted-wall study. Industrial & Engineering Chemistry Research 40, 2310-2321.

Fuller, E.N., Schettler, P.D., Giddings, J.C., 1966. A New Method for Prediction of Binary Gas-Phase Diffusion Coeffecients. Industrial and Engineering Chemistry 58, 19-27.

Gilliland, E.R., Sherwood, T.K., 1934. Diffusion of Vapors into Air Streams. Industrial & Engineering Chemistry 26, 516-523.

Goren, S.L., 1962. The instability of an annular layer thread of fluid. Journal of Fluid Mechanics 13, 309-319.

Grabbert, G., 1974. Theoretische und experimentelle Untersuchung des Stoffübergangs am Rieselfilm unter Berücksichtigung der Krümmung der Phasengrenzfläche (in German). Dissertation, Bergakademie Freiberg, Freiberg.

Grabbert, G., Wünsch, G., 1973. Zur Hydraulik stark gekrümmter Rieselfilme (in German). Freiberger Forschungshefte A 517, 61-83.

Grünig, J., Skale, T., Kraume, M., 2010. Liquid Flow on a Vertical Wire in a Countercurrent Gas Flow. Chemical Engineering Journal 164, 121-131.

Harvey, A.H., 1996. Semiempirical correlation for Henry's constants over large temperature ranges. AIChE Journal 42, 1491-1494.

Hattori, K., Ishikawa, M., Mori, Y.H., 1994. Strings of Liquid Beads for Gas-Liquid Contact Operations. AIChE Journal 40, 1983-1992.

Helbig, K., 2007. Messung zur Hydrodynamik und zum Wärmetransport bei der Filmverdampfung (in German). Dissertation, Technische Universität Darmstadt, Darmstadt.

Henstock, W.H., Hanratty, T.J., 1979. Gas Absorption by a Liquid Layer Flowing on the Wall of a Pipe. AIChE Journal 25, 122-131.

Hiby, J.W., 1968. Eine Fluoreszenzmethode zur Untersuchung des Transportmechanismus bei der Gasabsorption im Rieselfilm (in German). Wärme- und Stoffübertragung 1, 105-116.

Higbie, R., 1935. Rate of Absorption of a Pure Gas into a Still Liquid during Short Periods of Exposure. Transactions of the American Institute of Chemical Engineers 31, 365-389.

Hikita, H., Ishimi, K., 1987. A simplified method of estimating mass and heat transfer coefficients for turbulent gas streams in wetted-wall columns. Journal of Chemical Engineering of Japan 20, 185-188.

Jödecke, M., Schuch, G., Löning, J.-M., Shilkin, A., 2008. Verfahren zur Aufarbeitung eines Stoffgemisches (in German). Patent Application 1935486 A1.

Kliakhandler, I.L., Davis, S.H., Bankoff, S.G., 2001. Viscous beads on vertical fibre. Journal of Fluid Mechanics 429, 381-390.

Lel, V.V., Al-Sibai, F., Leefken, A., Renz, U., 2005. Local thickness and wave velocity measurement of wavy films with a chromatic confocal imaging method and a fluorescence intensity technique. Experiments in Fluids 39, 856-864.

Lin, S.P., Liu, W.C., 1975. Instability of Film Coating of Wires and Tubes. AIChE Journal 21, 775-782.

Maćkowiak, J.F., 1999. Untersuchungen des gas- und flüssigkeitsseitigen Stoffüberganges in Kolonnen mit strukturierten Packungen (in German). Chemie Ingenieur Technik 71, 100-104.

Migita, H., Soga, K., Mori, Y.H., 2005. Gas Absorption in a Wetted-Wire Column. AIChE Journal 51, 2190-2198.

Mouza, A.A., Vlachos, N.A., Paras, S.V., Karabelas, A.J., 2000. Measurement of liquid film thickness using a laser light absorption method. Experiments in Fluids 28, 355-359.

Nagaoka, T., Manteufel, R.P.C., 2003. Column packing and method for manufacturing the same. Patent Application EP 1155739 A3.

Nielsen, C.H.E., Kiil, S., Thomsen, H.W., Dam-Johansen, K., 1998. Mass transfer in wetted-wall columns: Correlations at high Reynolds numbers. Chemical Engineering Science 53, 495-503.

Nußelt, W., 1916. Die Oberflächenkondensation des Wasserdampfes (in German). Z. VDI 60, 541-546.

Pakdehi, S.G., Taheri, S., 2010. Separation of Hydrazine from Air by Wetted Wire Column. Chemical Engineering & Technology 33, 1687-1694.

Park, C.D., Nosoko, T., 2003. Three-Dimensional Wave Dynamics on a Falling Film and Associated Mass Transfer. AIChE Journal 49, 2715-2727.

Rayleigh, L., 1878. On the Instability of Jets. Proceedings of the London Mathematical Society s1-10, 4-13.

Rocha, J.A., Bravo, J.L., Fair, J.R., 1996. Distillation columns containing structured packings: A comprehensive model for their performance. 2. Mass-transfer model. Industrial & Engineering Chemistry Research 35, 1660-1667.

Spedding, P.L., Jones, M.T., 1988. Heat and mass transfer in wetted-wall columns: I. The Chemical Engineering Journal 37, 165-176.

Trifonov, Y.Y., 1992. Steady-State Traveling Waves on the Surface of a Viscous Liquid Film Falling Down on Vertical Wires and Tubes. AIChE Journal 38, 821-834.

Uchiyama, K., Migita, H., Ohmura, R., Mori, Y.H., 2003. Gas absorption into "string-of-beads" liquid flow with chemical reaction: application to carbon dioxide separation. International Journal of Heat and Mass Transfer 46, 457-468.

VDI-Wärmeatlas, 1994. Berechnungsblätter für den Wärmeübergang (in German), 7 ed. VDI-Verlag, Düsseldorf.

VDI/VDE Richtlinien, 2007. VDI 3514 Part 1: Measurement of humidity - Characteristics and symbols. Beuth Verlag, Berlin.

Vogelpohl, A., 2006. Vorrichtung zum Gas/Flüssigkeit-Stoffaustausch (in German). Patent Application 102005011228 A1.

Wilke, C.R., Chang, P., 1955. Correlation of Diffusion Coefficients in Dilute Solutions. AIChE Journal 1, 264-270.

Wohlfarth, C., Wohlfarth, B., 1997. Surface Tension of Pure Liquids and Binary Liquid Mixtures, 8 ed. Springer, Berlin.

Yoshimura, P.N., Nosoko, T., Nagata, T., 1996. Enhancement of mass transfer into a falling laminar liquid film by twig-dimensional surface waves - Some experimental observations and modeling. Chemical Engineering Science 51, 1231-1240.

Appendix

A: Calculation of the height of transfer unit HTU_g and HTU_l

It is convenient to use the mass transfer coefficient which is referred to the dry wire surface area so the effective film surface area does not have to be known. The height of a gas-side transfer unit is dependent on the packing density z_P:

$$HTU_g = \frac{v_g}{\beta_{g,dry} \cdot a_P} = \frac{v_g}{\beta_{g,dry} \cdot C_W z_P}. \quad (A.1)$$

The height of a liquid-side transfer unit does not depend on the packing density when it is referred to the individual liquid flow rate of the single wire:

$$HTU_l = \frac{\dot{N}_{l,W}}{\beta_{l,dry}\, c_l \cdot \tilde{a}_W} = \frac{\dot{V}_{l,W}}{\beta_{l,dry} \cdot C_W} = \frac{B_W}{\beta_{l,dry}}. \quad (A.2)$$

When considering the liquid load of the packing B_P the height of a liquid-side transfer unit can be written as

$$HTU_l = \frac{v_l}{\beta_{l,dry} \cdot a_P} = \frac{B_P}{\beta_{l,dry} \cdot C_W\, z_P}. \quad (A.3)$$

B: Conversion of absorption efficiency E into HTU_l

To compare our results with the single wire mass transfer data from Chinju et al. for the CO_2-water/air system which are given as absorption efficiency against the running length, a relation of the absorption efficiency and the HTU_l values is made.

The absorption efficiency is defined as

$$E = \frac{c - c_{in}}{c^* - c_{in}}, \qquad 1 - E = \frac{c^* - c}{c^* - c_{in}}. \quad (B.1)$$

A molar balance over the liquid film gives

$$0 = \dot{V}_{l,W}\mathrm{d}c + \beta \cdot \tilde{a}_{l,W}(c - c^*)\mathrm{d}z \ \text{ with } \ \mathrm{d}A = \tilde{a}_{l,W}\mathrm{d}z \quad (B.2)$$

$$\underbrace{\frac{\dot{V}_{\mathrm{l,W}}}{\beta \cdot \tilde{a}_{\mathrm{l,W}}}}_{HTU_{\mathrm{l}}} \underbrace{\int_{c_{\mathrm{in}}}^{c_{\mathrm{out}}} \frac{1}{c - c^{*}} \mathrm{d}c}_{NTU_{\mathrm{l}}} = \int_{z_{\mathrm{in}}}^{z_{\mathrm{out}}} \mathrm{d}z = H_{\mathrm{P}} \tag{B.3}$$

Assuming that c^* is constant over the height of the wire (low solubility of CO_2 in the liquid phase and sufficiently high gas flow rate) the integral can be written as

$$\int_{c_{\mathrm{in}}}^{c_{\mathrm{out}}} \frac{1}{c - c^{*}} \mathrm{d}c = \ln \underbrace{\frac{c_{\mathrm{out}} - c^{*}}{c_{\mathrm{in}} - c^{*}}}_{(1-E)} \tag{B.4}$$

This leads to the relations of NTU_{l} and HTU_{l} in dependency of E:

$$NTU_{\mathrm{l}} = \ln(1 - E) \qquad \text{and} \qquad HTU_{\mathrm{l}} = \frac{H_{\mathrm{P}}}{NTU_{\mathrm{l}}} = \frac{H_{\mathrm{P}}}{\ln(1 - E)} \tag{B.5}$$

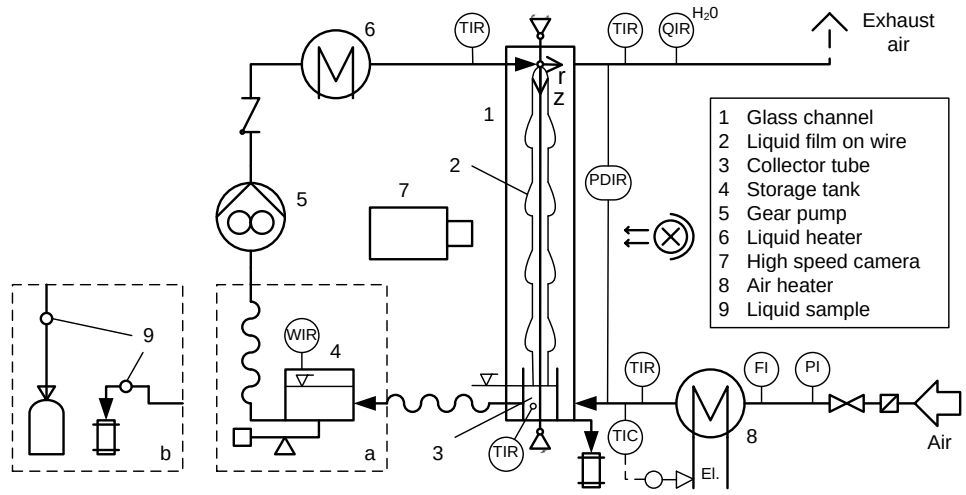

Fig. 1. Sketch of experimental set-up.

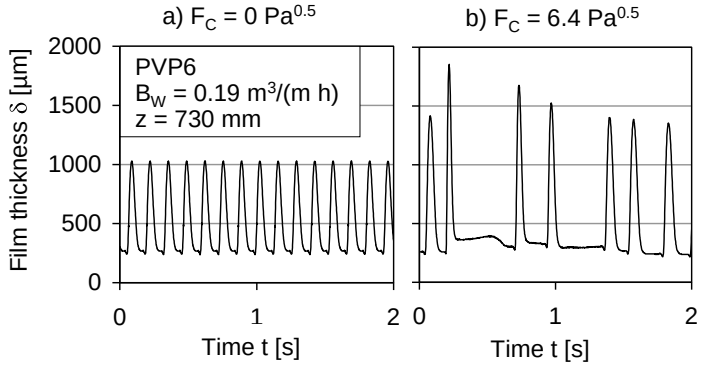

Fig. 2. Recording of the local film for a) no gas load and b) high gas load.

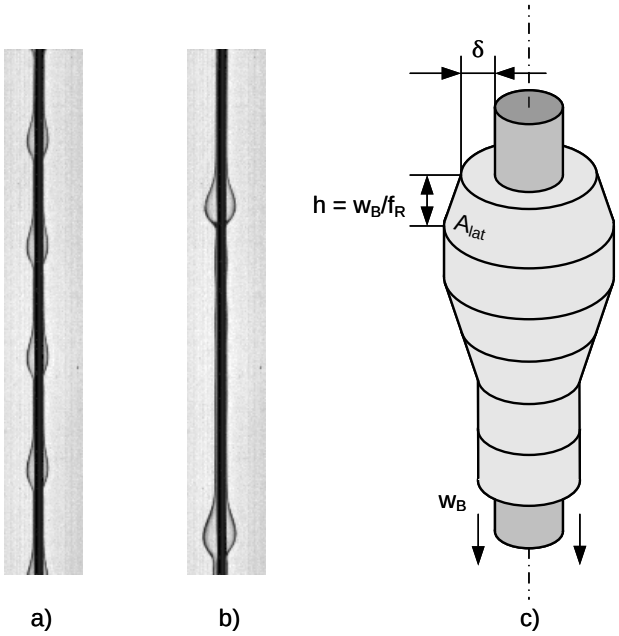

Fig. 3. Pictures of the liquid film of PVP6, B_W = 0.19 m^3/(m h) for a) no gas load and b) high gas load. c): Sketch of film volume model.

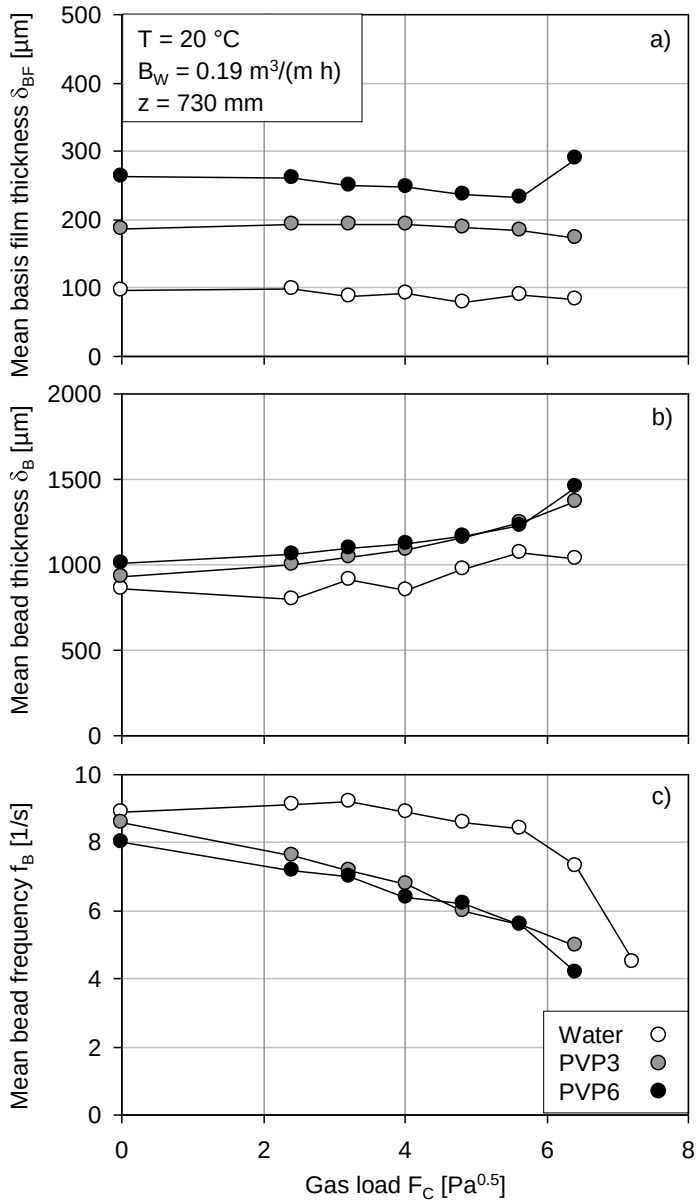

Fig. 4. Mean basis film thickness (a), mean bead thickness (b), and mean bead frequency (c) against the gas load for different liquids.

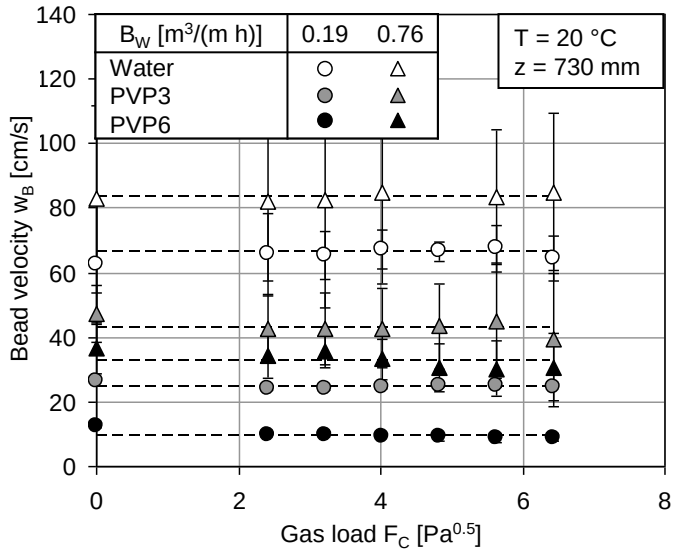

Fig. 5. Mean bead velocity depending on the gas load for different liquids and liquid loads.

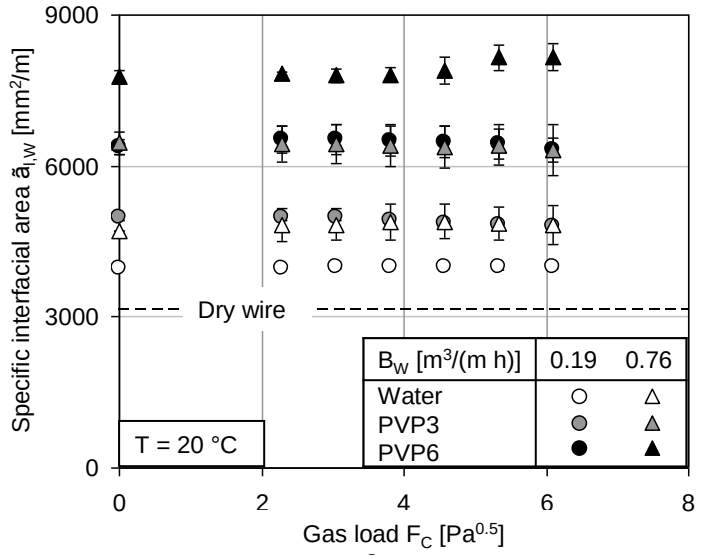

Fig. 6. Specific interfacial area depending on the gas load for different liquids and liquid loads.

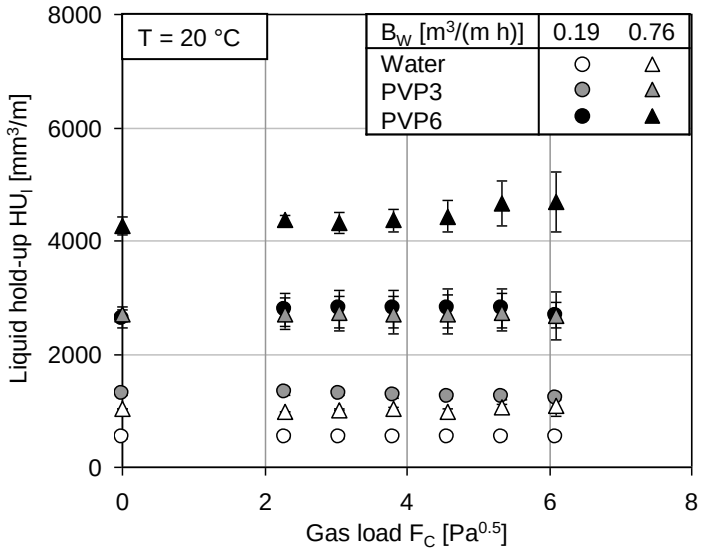

Fig. 7. Liquid hold-up depending on the gas load for different liquids and liquid loads.

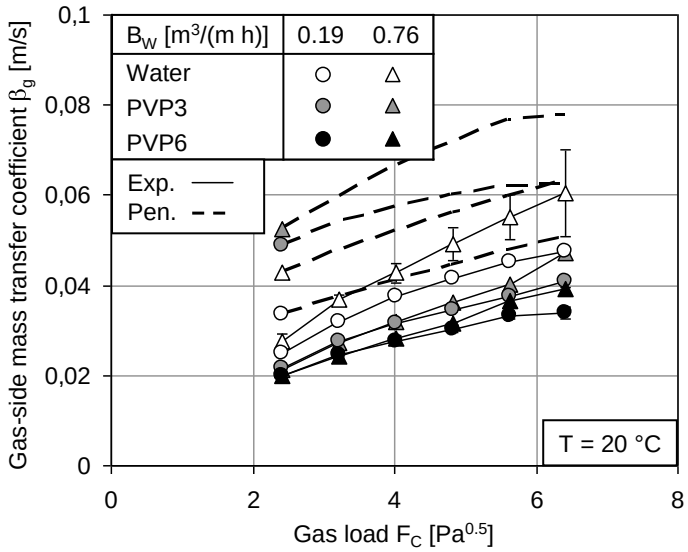

Fig. 8. Gas-side mass transfer coefficient depending on the gas load for different liquids and liquid loads. Experimental values are compared to theoretical values calculated with the penetration theory.

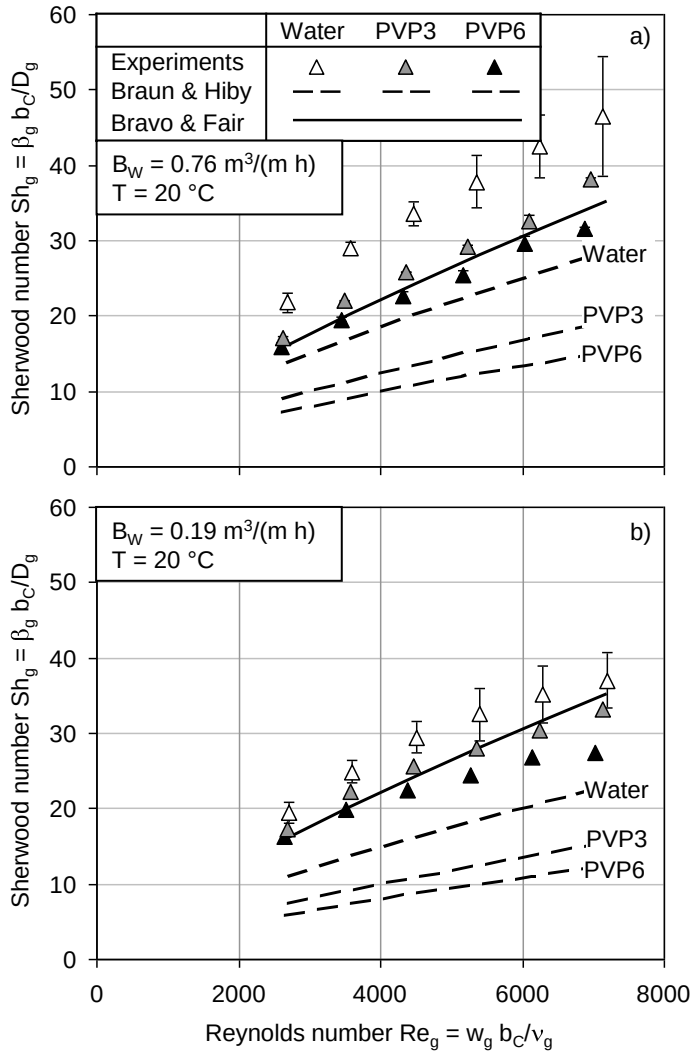

Fig. 9. Mean gas-side Sherwood number depending on the Reynolds number for different liquids and different liquid loads a) and b). Comparison with correlations for mass transfer in tubes (Braun and Hiby, 1970) and inside structured packings (Bravo and Fair, 1982).

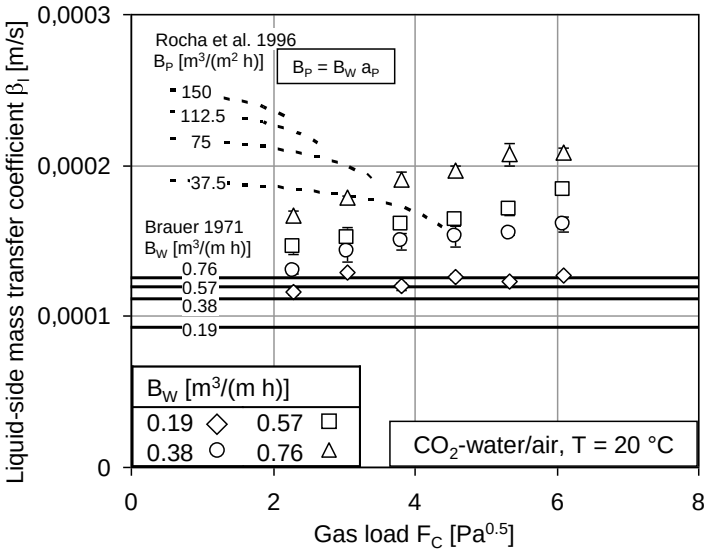

Fig. 10. Liquid-side mass transfer coefficient depending on the gas load for different liquid loads. Comparison with data derived from Brauer (1971) for planar films (independent from gas load) and the model of Rocha et al. (1996) for structured packings.

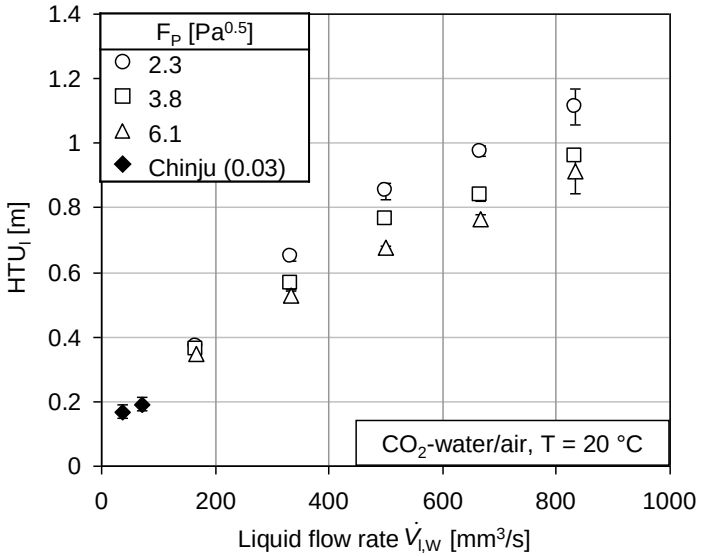

Fig. 11. HTU_l values for the single wire depending on the liquid flow rate for different gas loads. Comparison with data from Chinju et al. (2000).

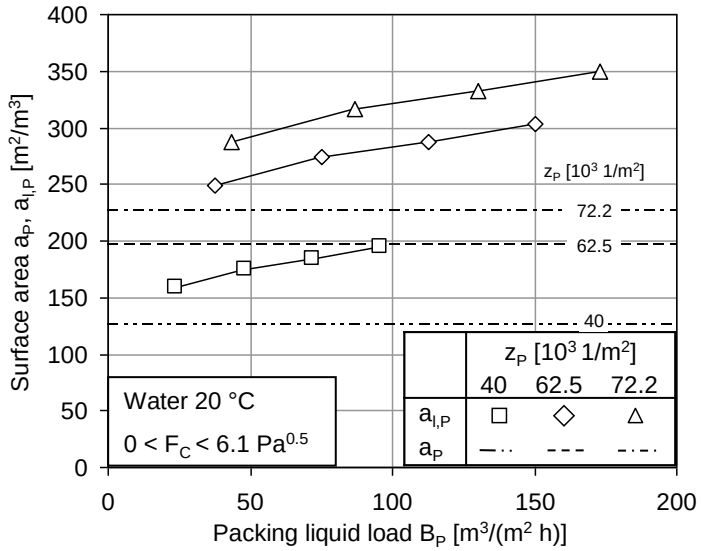

Fig. 12. Predicted effective film surface area depending on the packing liquid load for different wire packing densities.

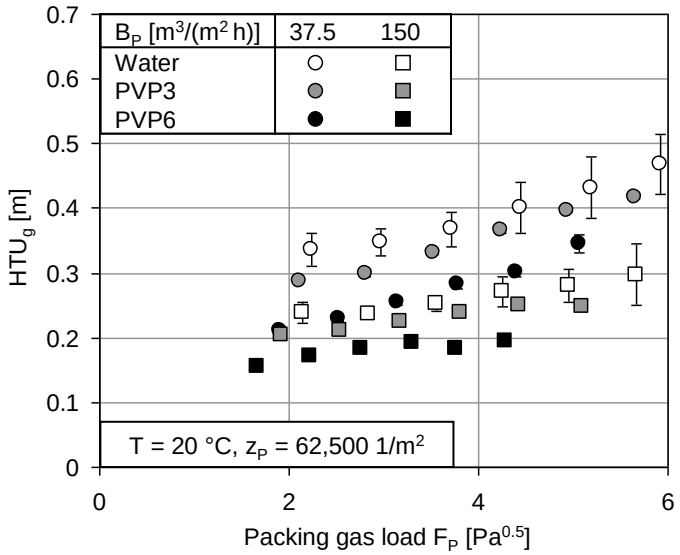

Fig. 13. Predicted HTU_g values depending on the gas load for different liquids and liquid loads and a defined wire packing density.

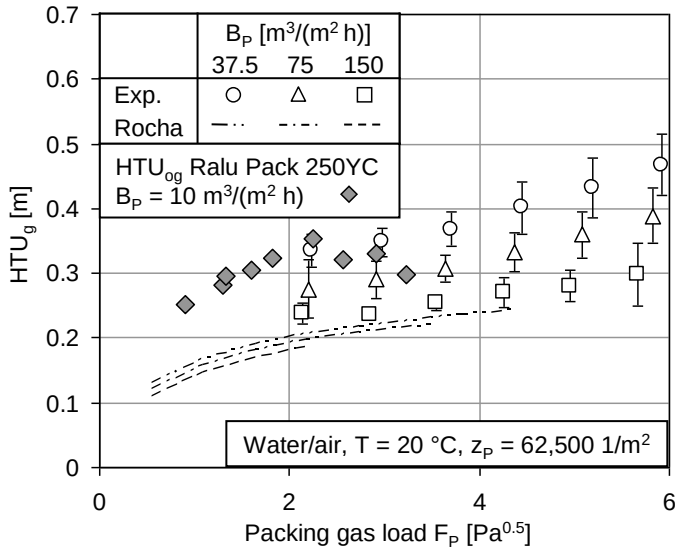

Fig. 14. Predicted HTU_g values of the packing depending on the gas load for different liquid loads for a defined wire packing density in comparison with literature data.

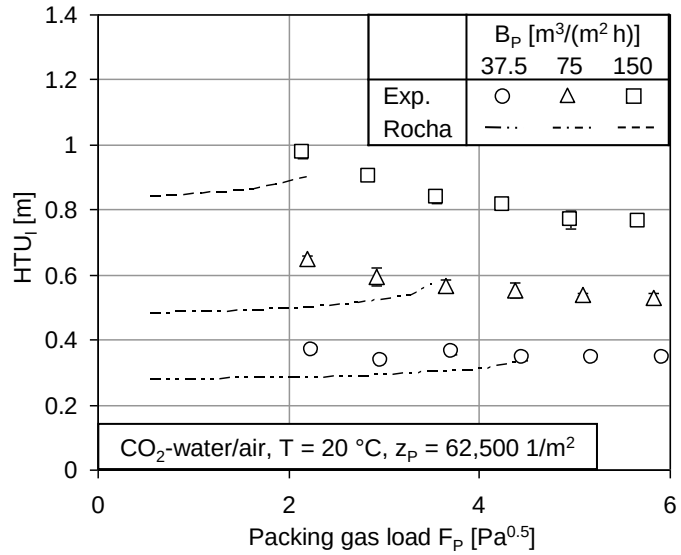

Fig. 15. Predicted HTU_l values depending on the gas load for different liquid loads. Comparison with the model of Rocha et al. (1996) with parameters $a_p = 200\ m^2/m^3$, $\varphi = 45\ °$.